Lynner, C., 2021, Anisotropy-revealed change in hydration along the Alaska subduction zone:
Geology, v. 49, https://doi.org/10.1130/G48860.1

Anisotropy-revealed change in hydration along the Alaska subduction zone

Colton Lynner[1*]

[1]Department of Earth Sciences, University of Delaware, Newark, DE

*Corresponding author: clynner@udel.edu

DR1. Table of Split shear wave splitting measurements

DR2. Table of Null shear wave splitting measurements

DR3. Table of station orientations.

Shear Wave Splitting

Shear wave splitting provides constraints on seismic anisotropy in the upper mantle and crust through the fast splitting direction and the delay time [Long and Silver, 2009]. When incoming shear waves interact with anisotropic earth materials, they split into two orthogonally propagating waves that travel at different velocities. The polarization of the faster traveling wave denotes the fast splitting direction and is directly related to the orientation of seismic anisotropy. The time delay between the fast and slow waves is the delay time and relates to both the strength of anisotropy and the layer thickness [Silver and Chan, 1991]. Shear wave splitting is a path integrated measurement sensitive to any anisotropy along each ray path, so splitting alone does not provide mineral source or depth information on anisotropy.

Layered Anisotropy

Multiple layers of anisotropy are likely present in subduction zones: including the sub-slab mantle, the subducting slab itself, the mantle wedge, and the upper plate. Along the AACSE, different stations are sensitive to different portions of the subduction system. OSNAP stations, for example, sample anisotropy in the subducting slab, overriding plate, and in the sub-slab mantle. OSNAP stations sample little-to-no mantle wedge material removing it as a potential influence on shear wave splitting. Constraining different layers of anisotropy with shear wave splitting requires sufficient backazimuthal coverage to model the impacts of 2 or 3 layers of anisotropy [Eakin and Long, 2013]. The high noise levels and short deployment time of the AACSE OBS instruments prevents sufficient coverage of shear wave splitting measurements to model multiple layers of anisotropy, with the majority of AACSE stations returning fewer than 3 measurements.

Previous source-side shear wave splitting measurements, which isolate anisotropy in the sub-slab mantle, show predominantly plate motion aligned splitting beneath the OSNAP stations, both in the Shumagin Gap and in the Semidi segment [Lynner and Long, 2014]. This suggests anisotropy in the sub-slab mantle does not greatly vary beneath the AACSE deployment, removing the sub-slab mantle as the source of the observed splitting change at OSNAP stations. Only the subducting slab and the upper plate, therefore, are the potential drivers of OSNAP splitting. I ascribe the change in OSNAP splitting to the subducting slab since it follows a known tectonic structural change that has previously been suggested to be well hydrated [Shillington et al., 2015]. With the existing splitting measurements, however, I cannot rule out the upper plate as a contributing, or the sole, source of the change in splitting at OSNAP stations. This will be the focus of a future study.

Other layers of anisotropy may exist along the margin. Stress-induced shape preferred anisotropy, for example, has been suggested to contribute to shear wave splitting at convergent margins with high coupling. Changes in interplate coupling between the Shumagin gap and the Semidi segment may lead to variations in stress-induced cracks and subsequent anisotropy. Stress-induced anisotropy, however, is unlikely to be the primary source of the change in anisotropy at OSNAP stations. Stress-induced anisotropy is typically restricted to the upper-crust, which produces ~0.1 to ~0.3 seconds of delay time [Crampin and Chastin, 2003]. This is far below the ~1.0s dt I observe at the OSNAP stations. Stress-induced anisotropy may play a role in the pattern of shear wave splitting along the margin but is unlikely the primary cause of the along strike change in splitting.

References

Crampin, S., and S. Chastin (2003), A review of shear wave splitting in the crack-critical crust, Geophysical Journal International, 155(1), 221–240. doi:10.1046/j.1365-246X.2003.02037.x.

Eakin, C.M. and M.D. Long, 2013, Complex anisotropy beneath the Peruvian flat slab from frequency-dependent, multiple-phase shear wave splitting analysis. Journal of Geophysical Research, *118*(9), 4794-4813. doi: 10.1016/j.epsl.2014.12.015

Long, M.D. and Silver, P.G., 2009, Shear wave splitting and mantle anisotropy: Measurements, interpretations, and new directions. Surv. Geophys. 30, 407–461. doi: 10.1007/s10712-009-9075-1

Lynner, C. and Long, M.D., 2014, Sub-slab anisotropy beneath the Sumatra and circum-Pacific subduction zones from source-side shear wave splitting observations. Geochemistry, Geophysics, Geosystems, 15, 2262-2281, doi:10.1002/2014GC005239

Shillington, D.J., et al., 2015, Link between plate fabric, hydration and subduction zone seismicity in Alaska. Nature Geoscience, 8(12), 961-964, doi: 10.1038/ngeo2586

Silver, P.G., and Chan, W.W., 1991, Shear wave splitting and subcontinental mantle deformation. Journal of Geophysical Research 96, 16429–16454. doi: 10.1029/91JB00899

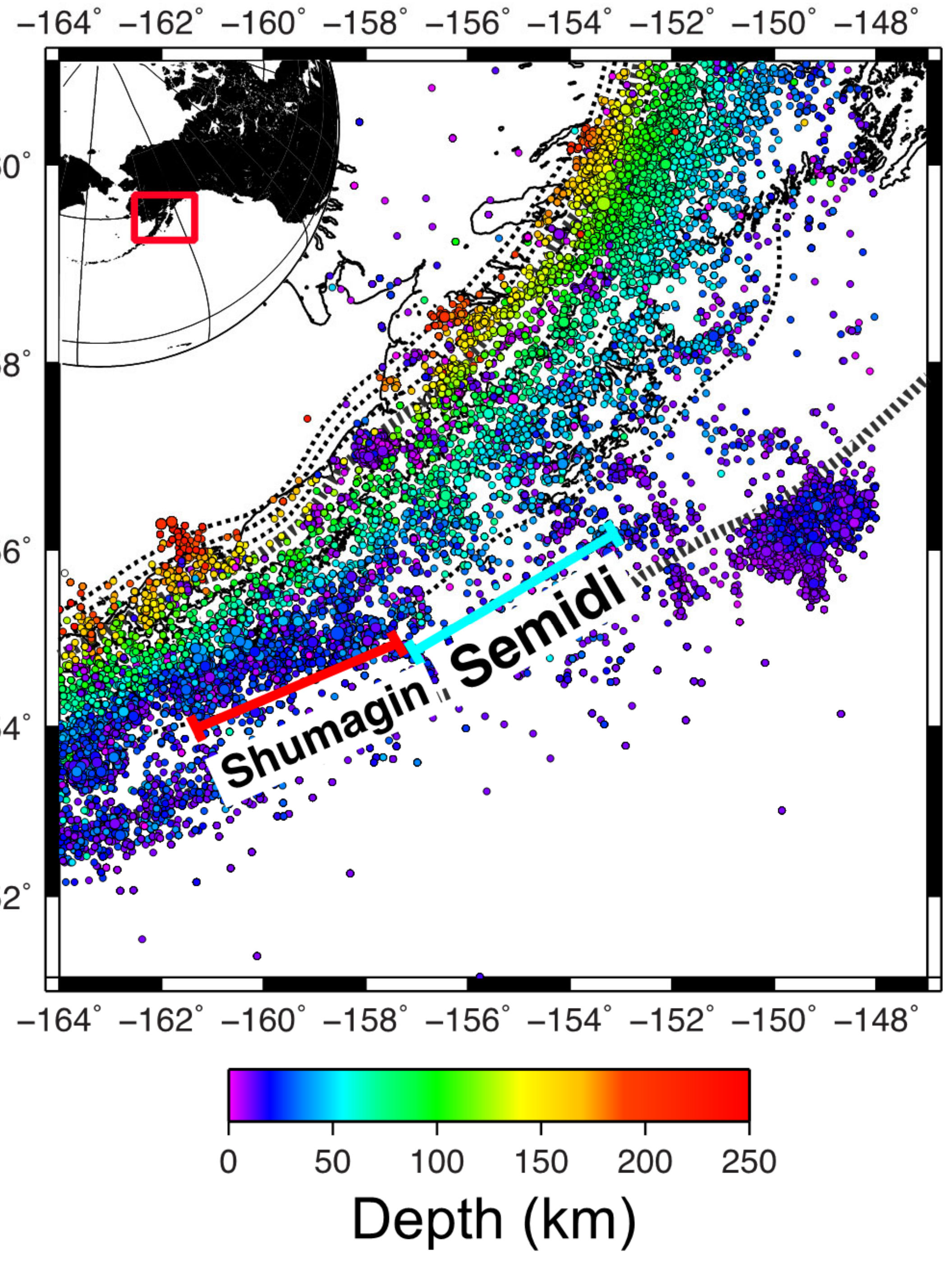

Figure S1. Seismicity along the Alaska-Aleutians subduction zone in the region of study from the National Earthquake Information Center (NEIC).

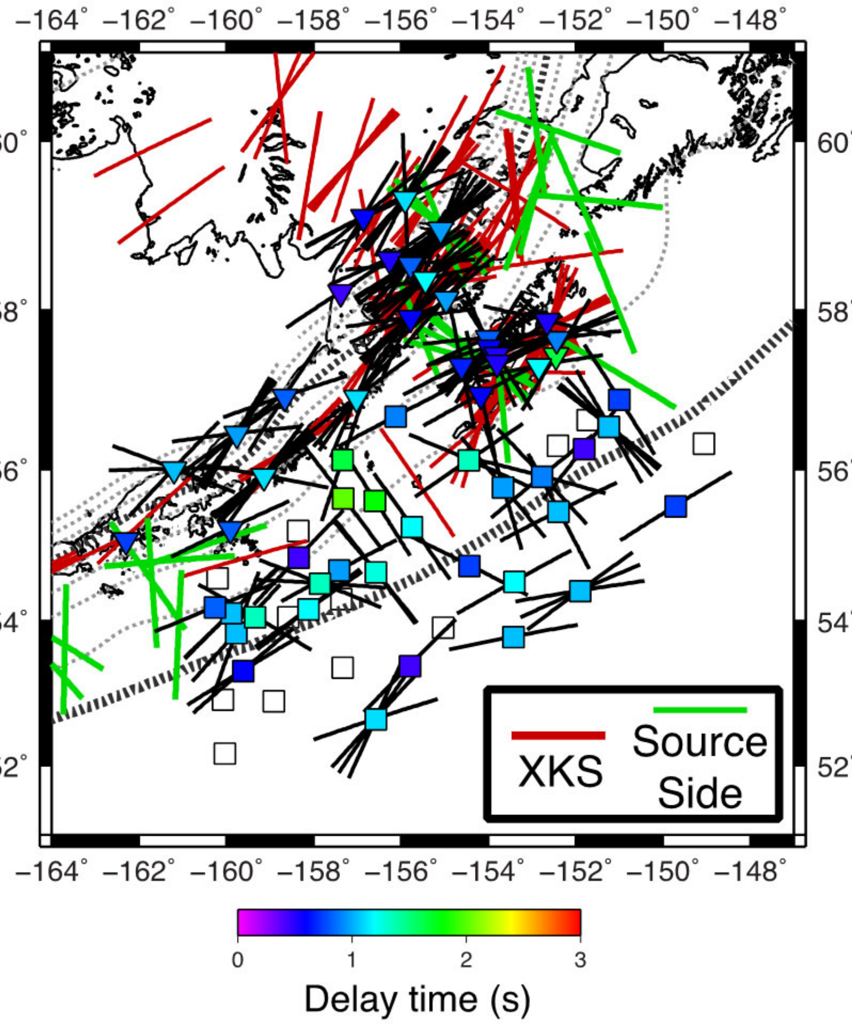

Figure S2. Individual shear wave splitting measurements at AACSE stations along with previous shear wave splitting measurements in the region [Hanna and Long, 2012; Lynner and Long, 2014; Venereau et al., 2019; McPherson, 2020]. Fast splitting directions for AACSE stations are shown by the orientation of the black bars. AACSE station averaged delay times are shown by the station color. Previous XKS splitting measurements are shown as red lines. Source-side measurements, which sample only the sub-slab mantle near the slab, are plotted in yellow.

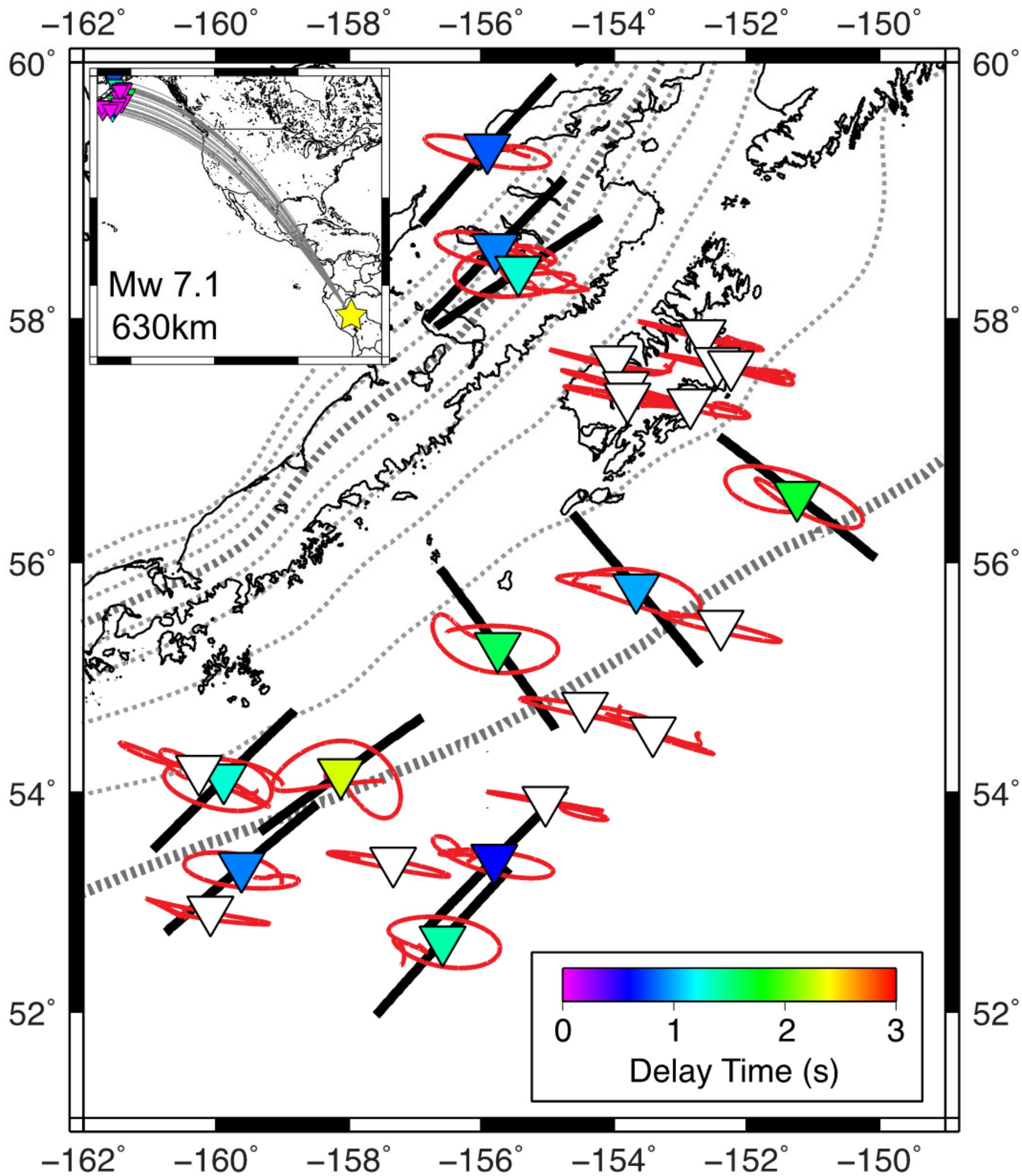

Figure S3. Shear wave splitting at AACSE stations recorded from a South American event on August 24th, 2018. Orientations of the black bars denote the measured fast splitting direction, and the symbol color shows the measured delay time. White stations represent a null measurement. Particle motions of each measurement are shown. Split measurements are characterized by elliptical particle motions, while null measurements have linear particle motions.

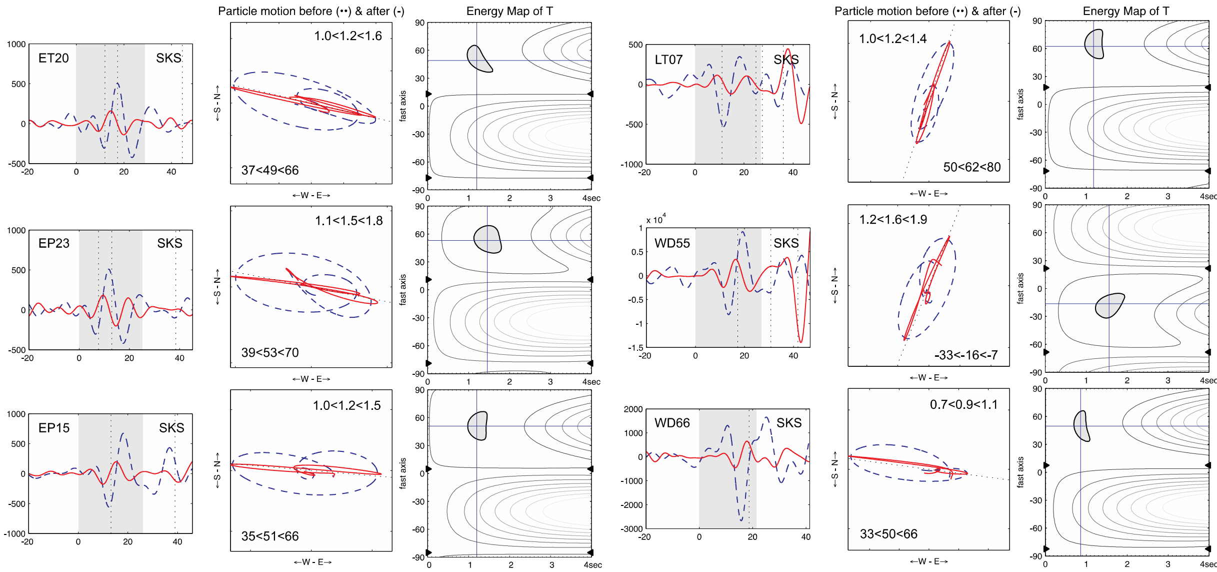

Figure S4. Examples of individual splitting measurements at 6 AACSE stations. (left) Plots of radial (blue) and transverse (red) components for each measurement. The measurement window is highlighted for each. (middle) Initial (blue) and corrected (red) particle motions for the splitting measurements. The resultant fast direction and delay time with associated error bounds are shown in the top and bottom, respectively. (right) Error space plots of the splitting measurements with the 2σ error spaces highlighted. Well resolved split measurements are apparent for several fast directions suggesting the observed differences in splitting directions across AACSE are robust.

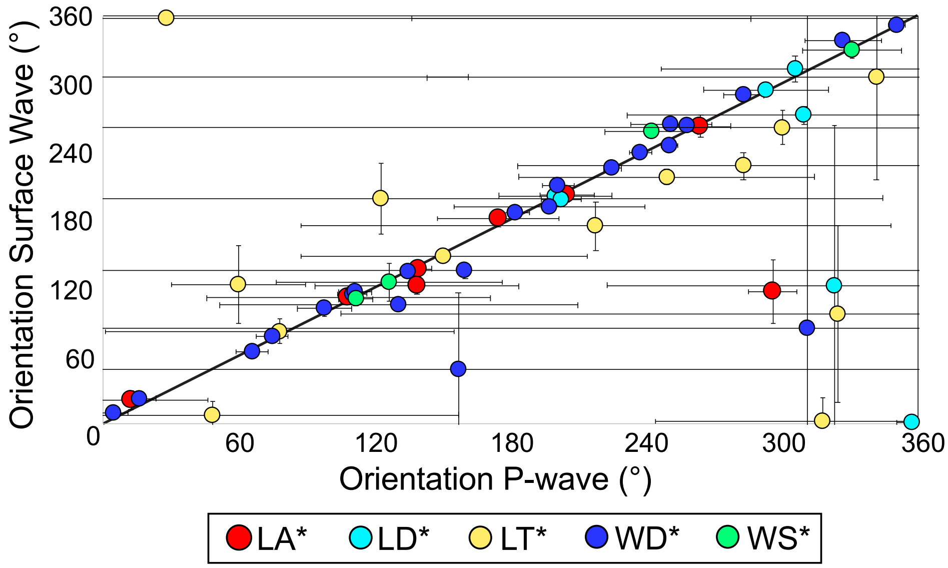

Figure S5. Calculated orientations for each of the AACSE OBS stations using Rayleigh wave [Braunmiller et al., 2020] and P-wave [Doran and Laske, 2017] polarizations with associated errors for the different instrument types. While the calculated orientations typically agree, the surface waves provided better resolved orientations.

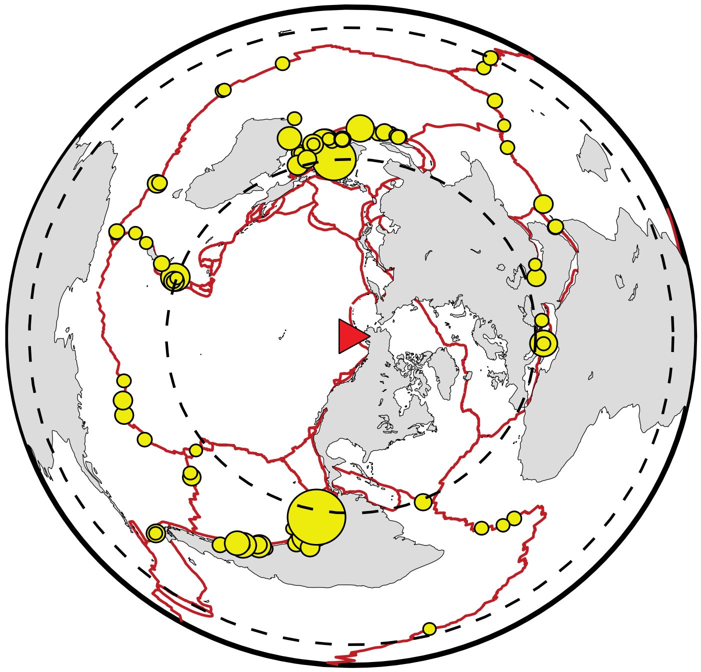

Figure S6. Map of the earthquakes used in this study.

Table DR1

Splits

Station	Station Lat (°)	Station Lon (°)	Event Lat (°)	Event Lon (°)	Depth (km)	Backazimuth (°)	Distance (°)	Phase	FD Low Bound (°)	Fast Direction (FD)(°)	FD Up Bound (°)	DT Low Bound (s)	Delay Time (DT) (s)	DT Up Bound (s)
WP30	56.001	-161.2014	-8.3	116.4	34	259.1	92.6	SKS	-79.9	-68.9	-61.7	1.5	1.8	2.1
WP30	56.001	-161.2014	-2	98.6	9	277.4	97.4	SKS	31.3	43.4	59.7	0.9	1.2	1.5
WP30	56.001	-161.2014	-57.4	-66.4	10	129	136.4	PKS	61.7	89	-71.8	0.7	1.2	2
WS75	54.17963	-160.256908	0.4	97.7	19	280	96.7	SKS	53.6	68	81.9	0.8	1.1	1.5
WS27	55.2236	-159.9136	-2.9	100.1	20	276.6	98	SKS	49.6	64.6	75.8	0.9	1.1	1.5
LD45	54.1025	-159.8829	-11	-70.8	630	97.3	98.4	SKS	29.3	45.3	65.7	0.9	1.3	1.8
LD45	54.1025	-159.8829	0.4	97.7	19	280.3	96.9	SKS	29.3	46.3	69.8	0.8	1.4	2.2
LD44	53.8302	-159.7736	-8.2	116.5	14	260.1	93	SKS	9.1	20.1	37.4	1.3	1.9	2.7
LD44	53.8302	-159.7736	-7.3	104.8	49	270.1	99.1	SKS	13.1	42.1	77.9	0.5	0.8	1.9
WP25	56.453	-159.7563	-8.2	116.5	14	260.2	93.4	SKS	19.2	30.2	45.5	1.5	1.9	2.4
WP25	56.453	-159.7563	-10.4	119	24	257	93.9	SKS	3	33	61.7	0.6	0.9	1.6
WP25	56.453	-159.7563	-7.3	104.8	49	270.5	99.1	SKS	25.3	36.5	49.6	1.1	1.4	1.7
WP25	56.453	-159.7563	0.4	97.7	19	280.7	96.6	SKS	33.4	48.7	71.8	0.7	0.9	1.3
WP25	56.453	-159.7563	-2	98.6	9	278.6	98.1	SKS	41.5	54.6	69.8	1.2	1.6	2
WP25	56.453	-159.7563	-57.4	-66.4	10	129.3	136	PKS	57.6	83.3	-71.8	0.6	0.8	1.4
WD66	53.31452	-159.617565	-11	-70.8	630	97.6	98.1	SKS	33.4	49.6	65.7	0.7	0.9	1.1
WD66	53.31452	-159.617565	0.4	97.7	19	280.4	97.2	SKS	31.3	58.4	83.9	0.5	0.6	1
WD52	54.046622	-159.346215	-7.4	119.8	529	258.3	90.6	SKS	-73.8	-59.7	-45.5	1.2	1.8	2.3
WS26	55.9123	-159.1431	-29.9	-112	19	140.3	94.7	SKS	81.9	-79.7	-65.7	1	1.4	1.9
WS26	55.9123	-159.1431	-8.2	116.5	14	260.7	93.7	SKS	9.1	36.7	63.7	0.7	1	1.6
WS26	55.9123	-159.1431	-7.3	104.8	49	270.9	99.4	SKS	37.4	42.9	51.6	1.3	1.5	1.6
WS26	55.9123	-159.1431	0.4	97.7	19	281.2	97	SKS	41.5	45.2	49.6	1.6	1.8	2
WS26	55.9123	-159.1431	-2.9	100.1	20	277.4	98.4	SKS	39.4	49.4	61.7	1.6	2	2.4
WS26	55.9123	-159.1431	-7.3	104.8	49	270.9	99.4	SKKS	35.4	52.9	65.7	1	1.3	1.6
WP24	56.9241	-158.6603	-8.1	-71.6	570	96.9	95.2	SKS	23.3	32.9	49.6	1.1	1.7	2.4
WP24	56.9241	-158.6603	-31.8	-179.4	115	197.5	90.4	SKS	45.5	71.5	-90	0.4	0.5	1
LT13	54.8439	-158.3466	-7.3	104.8	49	271.4	99.9	SKS	15.2	43.4	73.8	0.4	0.6	1.2
LA33	54.1528	-158.1143	-8.1	-71.6	570	97.6	94.6	SKS	21.2	51.6	79.9	0.6	0.9	1.6
LA33	54.1528	-158.1143	-11	-70.8	630	98.7	97.3	SKS	35.4	54.7	75.8	1.4	2.3	3.2
LA32	54.4982	-157.8522	10.9	57.2	10	323.5	108.3	SKS	69.8	-86.5	-63.7	0.6	1	1.7
LA32	54.4982	-157.8522	-10.5	120.2	26	257.4	93.9	SKS	-75.8	-68.6	-67.8	2.2	2.5	2.9
LA30	54.6727	-157.4203	-5.8	-75.3	123	99.8	90.2	SKS	41.5	61.8	79.9	1	1.3	1.8
EP21	58.212	-157.3769	0.4	97.7	19	282.9	97.5	SKS	31.3	56.9	86	0.4	0.6	0.9
LT11	56.1202	-157.3355	14.1	51.7	10	330.7	105.7	SKKS	3	18.7	35.4	1.7	2.2	2.8
LT10	55.6251	-157.3251	0.2	97	9	283.2	98.6	SKKS	-45.5	-36.8	-31.3	2.3	2.7	3.1
EP23	56.9071	-157.0201	-10.4	119	24	259.3	95.4	SKS	11.1	23.3	41.5	0.8	1	1.3
EP23	56.9071	-157.0201	-10.3	119.2	26	259.2	95.3	SKS	9.1	35.2	59.7	0.8	1.3	2
EP23	56.9071	-157.0201	-2.9	100.1	20	279.3	99.4	SKS	29.3	41.3	57.6	1.4	2.2	2.9
EP23	56.9071	-157.0201	-2	98.6	9	281	99.5	SKS	39.4	53	69.8	1.1	1.5	1.8
EP16	59.1126	-156.8567	-7.3	104.8	49	273.4	100.5	SKS	19.2	31.4	55.6	0.4	0.6	1
EP16	59.1126	-156.8567	-8.1	-71.6	570	98.2	94.6	SKS	21.2	50.2	86	0.5	0.7	1.6
EP16	59.1126	-156.8567	-19.6	-69.3	102	102.3	105.5	SKKS	45.5	62.3	79.9	0.9	1.2	1.7

EP16	59.1126	-156.8567	-2	98.6	9	281.5	99.2	SKS	31.3	63.5	88	0.5	0.7	1.5
LT08	55.5883	-156.5975	-2.9	100.1	20	279.5	99.9	SKS	-55.6	-32.5	-15.2	1.6	2.4	3.2
WD60	52.644867	-156.579823	-7.1	122.7	578	258.3	90	SKS	11.1	24.3	41.5	1.3	1.9	2.6
WD60	52.644867	-156.579823	-7.3	104.8	49	272.4	101	SKS	21.2	34.4	57.6	0.7	1.1	1.6
WD60	52.644867	-156.579823	-11	-70.8	630	100.1	96.2	SKS	27.3	42.1	69.8	0.8	1.4	2.3
WD60	52.644867	-156.579823	-14.7	-70.2	267	101.8	99.5	SKS	47.5	71.8	86	0.8	1.4	2.2
WD61	54.647613	-156.579823	-8.2	116.5	14	262.7	94.9	SKS	-73.8	-39.3	-23.3	0.7	1.1	2.1
WD61	54.647613	-156.579823	-30.1	-72.1	11	112.5	111.1	SKS	-49.6	-37.5	-25.3	1.5	2.2	2.8
ET17	58.6097	-156.265	-8.1	-71.6	570	98.8	94.2	SKS	29.3	54.8	81.9	0.5	0.6	1
ET17	58.6097	-156.265	-14.7	-70.2	267	101	100.5	SKS	33.4	67	88	0.5	0.7	1.3
LT07	56.6712	-156.1199	-32	-177.9	29	198.3	90.6	SKS	49.6	62.3	79.9	1	1.2	1.4
EP14	59.3257	-155.9036	-0.3	-19.2	10	47.8	112.1	SKS	-35.4	-2.2	33.4	0.3	0.5	1.3
EP14	59.3257	-155.9036	-8.8	114.5	80	265.1	97.4	SKKS	19.2	27.1	35.4	1.7	2.1	2.5
EP14	59.3257	-155.9036	-10.3	119.2	26	260.4	96.3	SKS	27.3	36.4	47.5	1.6	2	2.3
EP14	59.3257	-155.9036	-8.8	114.5	80	265.1	97.4	SKS	25.3	39.1	51.6	1.2	1.6	1.9
EP14	59.3257	-155.9036	-11	-70.8	630	99.9	97	SKS	23.3	41.9	73.8	0.5	0.8	1.3
EP14	59.3257	-155.9036	-10.4	119	24	260.5	96.5	SKS	27.3	42.5	57.6	1.2	1.5	2
EP14	59.3257	-155.9036	-30	-71.4	63	110.7	112.9	SKS	41.5	64.7	-92	1	1.7	2.5
WD59	53.383713	-155.799387	-11	-70.8	630	100.6	95.9	SKS	23.3	44.6	81.9	0.4	0.6	1.3
ET18	58.5458	-155.788	-10.8	124.2	14	255.9	94	SKS	13.1	33.9	51.6	0.9	1.2	1.7
ET18	58.5458	-155.788	-7.3	104.8	49	274.2	101.1	SKS	35.4	42.2	55.6	1.2	1.4	1.6
ET18	58.5458	-155.788	-11	-70.8	630	100.1	96.8	SKS	25.3	44.1	79.9	0.6	0.9	1.6
ET18	58.5458	-155.788	-2	98.6	9	282.4	99.8	SKS	35.4	52.4	75.8	1	1.4	2
ET18	58.5458	-155.788	-19.6	-69.3	102	103.4	104.8	SKKS	41.5	57.4	75.8	0.9	1.2	1.5
ET18	58.5458	-155.788	-14.7	-70.2	267	101.4	100.3	SKS	27.3	59.4	88	0.5	0.7	1.3
ET18	58.5458	-155.788	-57.4	-66.4	10	129.5	135.7	PKS	51.6	85.5	-65.7	0.3	0.6	1.4
EP22	57.9007	-155.7865	-8.8	114.5	80	265.1	97.3	SKS	11.1	25.1	49.6	0.6	0.9	1.4
EP22	57.9007	-155.7865	-7.1	122.7	578	259	91.5	SKS	5.1	37	65.7	0.5	0.9	1.8
EP22	57.9007	-155.7865	-7.3	104.8	49	274.1	101.2	SKS	19.2	44.1	75.8	0.5	0.7	1.4
EP22	57.9007	-155.7865	0.4	97.7	19	284.3	98.4	SKS	35.4	48.3	69.8	0.7	1	1.4
EP22	57.9007	-155.7865	-2	98.6	9	282.3	100	SKS	27.3	50.3	86	0.5	0.7	1.4
EP22	57.9007	-155.7865	-14.7	-70.2	267	101.6	100.1	SKS	33.4	67.6	88	0.5	0.7	1.2
EP22	57.9007	-155.7865	-57.5	-66.3	10	130.1	135.4	PKS	61.7	82.1	-75.8	0.6	0.8	1.2
LD36	55.2524	-155.7525	-11	-70.8	630	100.5	96.2	SKS	-55.6	-35.5	-19.2	1.2	1.6	2.1
ET19	58.3686	-155.4394	-2.9	100.1	20	280.9	100	SKS	33.4	42.9	59.7	1	1.3	1.7
ET19	58.3686	-155.4394	-7.3	104.8	49	274.5	101.3	SKS	33.4	50.5	67.8	0.9	1.2	1.5
ET19	58.3686	-155.4394	-11	-70.8	630	100.4	96.6	SKS	31.3	56.4	81.9	0.9	1.3	2
ET19	58.3686	-155.4394	-2	98.6	9	282.6	100	SKS	39.4	60.6	79.9	0.9	1.3	1.8
ET19	58.3686	-155.4394	-8.1	-71.6	570	99.5	93.7	SKS	71.8	77.5	83.9	2.4	3.1	3.8
EP15	58.9664	-155.0867	-10.8	124.2	14	256.5	94.5	SKS	9.1	20.5	39.4	0.9	1.2	1.6
EP15	58.9664	-155.0867	-8.8	114.5	80	265.8	97.8	SKS	15.2	27.8	45.5	1.2	1.8	2.4
EP15	58.9664	-155.0867	-7.1	122.7	578	259.7	92.1	SKS	11.1	33.7	55.6	0.8	1.1	1.6
EP15	58.9664	-155.0867	-8.3	116.4	34	264.4	96.3	SKS	27.3	40.4	55.6	1.1	1.4	1.7
EP15	58.9664	-155.0867	-10.4	119	24	261.1	96.8	SKS	17.2	43.1	63.7	0.8	1.3	2
EP15	58.9664	-155.0867	-8.2	116.5	14	264.4	96.2	SKS	25.3	48.4	67.8	1.2	1.8	2.7

EP15	58.9664	-155.0867	-7.3	104.8	49	274.9	101.5	SKS	35.4	50.9	65.7	1	1.2	1.5
EP15	58.9664	-155.0867	-2.9	100.1	20	281.3	100.1	SKS	27.3	55.3	86	0.6	0.9	1.6
ET20	58.1304	-154.9716	-7.3	104.8	49	274.9	101.6	SKS	27.3	40.9	59.7	1	1.4	1.9
ET20	58.1304	-154.9716	-2	98.6	9	283	100.3	SKS	37.4	49	65.7	1	1.2	1.6
KD12	57.313	-154.6122	-31.8	-179.4	115	200.9	91.5	SKS	-29.3	-11.1	-3	1	1.2	1.6
KD12	57.313	-154.6122	-2	98.6	9	283.2	100.7	SKS	31.3	63.2	88	0.4	0.5	1
LT04	56.1118	-154.4446	14.2	51.6	10	333.6	106.4	SKS	-90	-66.4	-51.6	1.4	1.9	2.6
LT04	56.1118	-154.4446	-32	-177.9	29	199.7	90.4	SKS	35.4	55.7	83.9	1	1.7	2.8
WD57	54.736387	-154.434305	-10.8	124.2	14	256.8	93.9	SKS	-86	-63.2	-41.5	0.7	1	1.4
KS13	56.9472	-154.1729	-31.8	-179.4	115	201.2	91.2	SKS	-41.5	-12.8	1	0.6	0.8	1.2
KS13	56.9472	-154.1729	-2	98.6	9	283.5	101	SKS	31.3	61.5	-92	0.5	0.7	1.4
KT06	57.6517	-154.0041	-2.9	100.1	20	282	100.9	SKS	53.6	66	77.9	0.9	1.1	1.3
KT06	57.6517	-154.0041	-57.4	-66.4	10	131.1	134.4	PKS	57.6	85.1	-65.7	0.6	1	1.8
KT07	57.5375	-153.9814	-30.5	-177.8	30	200.4	90.3	SKS	-55.6	-23.6	3	0.5	0.7	1.2
KT07	57.5375	-153.9814	-10.6	120.2	29	260.8	96.7	SKS	15.2	30.8	49.6	1.2	1.7	2.3
KT07	57.5375	-153.9814	-7.3	104.8	49	275.6	102.2	SKS	23.3	41.6	67.8	0.4	0.5	0.9
KT07	57.5375	-153.9814	-2.9	100.1	20	282	100.9	SKS	33.4	50	75.8	0.6	0.7	1.1
KT07	57.5375	-153.9814	0.4	97.7	19	285.8	99.4	SKS	53.6	73.8	86	0.5	0.6	0.8
KT08	57.443	-153.8149	-31.8	-179.4	115	201.5	91.8	SKS	-59.7	-32.5	-1	0.5	0.7	1.4
KT08	57.443	-153.8149	0.4	97.7	19	285.9	99.5	SKS	35.4	57.9	81.9	0.5	0.6	1
KT08	57.443	-153.8149	-57.4	-66.4	10	131.4	134.2	PKS	55.6	69.4	-83.9	0.6	0.9	1.5
KT09	57.348	-153.7945	-19.6	-69.3	102	105.3	103.5	SKS	31.3	63.3	-92	0.4	0.6	1.2
KT09	57.348	-153.7945	0.4	97.7	19	285.9	99.5	SKS	39.4	67.9	88	0.5	0.7	1.2
WD55	55.761625	-153.662817	-11	-70.8	630	102.1	95.1	SKS	-65.7	-39.9	-11.1	0.7	1	2
WD55	55.761625	-153.662817	-31.8	-179.4	115	201.6	90.2	SKS	-33.4	-16.4	-7.1	1.2	1.6	1.9
WD53	53.779448	-153.422908	-30.1	-72.1	11	115.1	109.1	SKS	51.6	79.1	-83.9	0.9	1.4	2.3
LD41	54.5219	-153.4074	-30.1	-72.1	11	114.9	109.4	SKS	41.5	60.9	-92	0.9	1.5	2.4
LD41	54.5219	-153.4074	-30.1	-72.1	11	114.9	109.4	SKKS	43.5	60.9	88	1	1.7	2.6
KD04	57.3042	-152.8497	-30	-71.4	63	113.9	110.6	SKS	71.8	79.9	88	1.3	1.6	1.9
WD51	55.905087	-152.771768	10.9	57.2	10	328.8	108.7	SKS	71.8	-75.2	-45.5	0.4	0.7	1.5
WD51	55.905087	-152.771768	-18.2	120.4	10	257	103.3	SKKS	-71.8	-43	-29.3	1	1.7	2.7
WD51	55.905087	-152.771768	0.4	97.7	19	286.6	100.5	SKS	33.4	50.6	77.9	0.7	1.2	1.9
KD02	57.8618	-152.6575	10.9	57.2	10	329.2	107.1	SKS	73.8	-76.8	-49.6	0.5	0.7	1.4
KD00	57.4413	-152.4484	-35.7	-17.2	10	73.3	143.4	PKS	15.2	31.3	47.5	1.6	2.2	2.8
KD01	57.6401	-152.4375	-7.3	104.8	49	276.9	103	SKS	37.4	64.9	81.9	0.5	0.6	1
KD01	57.6401	-152.4375	-57.5	-66.3	10	132	133.9	PKS	61.7	70	88	0.9	1.3	1.7
KD01	57.6401	-152.4375	-30.1	-72.1	11	114.6	110.2	SKS	61.7	82.6	-86	1	1.6	2.2
WD50	55.449527	-152.391763	-8.1	-71.6	570	102.2	91.5	SKKS	-47.5	-27.8	-13.1	1.3	2	2.7
WD50	55.449527	-152.391763	-30.1	-72.1	11	115.3	109.3	SKS	37.4	63.3	-83.9	0.5	0.8	1.7
WD49	54.399083	-151.89947	-30	-71.4	63	115.5	108.9	SKS	41.5	53.5	71.8	1	1.5	2.3
WD49	54.399083	-151.89947	-30.1	-72.1	11	116	108.6	SKS	39.4	66	-86	0.5	0.9	1.8
WD49	54.399083	-151.89947	-34.2	-72.3	25	118.9	111.7	SKS	57.6	80.9	-83.9	1.2	1.8	2.6
WS72	56.257748	-151.81063	-8.2	116.5	14	266.8	97.8	SKS	5.1	38.8	77.9	0.3	0.6	1.7
WD70	56.541073	-151.234407	-11	-70.8	630	104	94	SKS	-61.7	-52	-41.5	1.3	1.7	2.3
WD70	56.541073	-151.234407	-8.2	116.5	14	267.3	98.1	SKS	-83.9	-48.7	-17.2	0.5	1	2.1

WD70	56.541073	-151.234407	-8.8	114.5	80	268.7	99.7	SKS	-65.7	-41.3	-23.3	1.1	1.7	2.4
WD70	56.541073	-151.234407	0.4	97.7	19	288	101.1	SKS	-49.6	-30	-7.1	0.7	1.1	1.5
LA39	56.8827	-151.0011	-14.7	-70.2	267	105.6	97.4	SKS	-61.7	-32.4	-3	0.6	1	1.7
WD46	55.521393	-149.703732	-0.2	119.8	20	270.2	90.5	SKS	43.5	58.2	71.8	0.8	1	1.4